The first large area, high x-ray energy phase contrast prototype for enhanced detection of threat object in baggage screening

Alberto Astolfo*[a], Marco Endrizzi[a], Benjamin Price[b], Ian Haig[b], Alessandro Olivo[a]

[a] Department of Medical Physics and Bioengineering, University College London, Malet Place, Gower Street, London WC1E 6BT, United Kingdom;
[b] X-Tek Systems-Nikon, Tring Business Centre, Icknield Way, Tring, Hertfordshire

ABSTRACT

X-ray imaging is the most commonly used method in baggage screening. Conventional x-ray attenuation (usually in dual-energy mode) is exploited to discriminate threat and non-threat materials: this is essentially, a method that has seen little changes in decades. Our goal is to demonstrate that x-rays can be used in a different way to achieve improved detection of weapons and explosives. Our approach involves the use of x-ray phase contrast and it a) allows much higher sensitivity in the detection of object edges and b) can be made sensitive to the sample's microstructure. We believe that these additional channels of information, alongside conventional attenuation which would still be available, have the potential to significantly increase both sensitivity and specificity in baggage scanning.

We obtained preliminary data demonstrating the above enhanced detection, and we built a scanner (currently in commissioning) to scale the concept up and test it on real baggage. In particular, while previous X-ray phase contrast imaging systems were limited in terms of both field of view (FOV) and maximum x-ray energy, this scanner overcomes both those limitations and provides FOVs up to 20 to 50 cm^2 with x-ray energies up to 100 keV.

Keywords: security, baggage screening, x-ray phase contrast, edge-illumination, dark-field imaging, multimodal imaging

1. INTRODUCTION

X-ray imaging is an established method for baggage screening and security inspections. The capability of x-rays to penetrate thick and dense materials allows identifying threat objects while avoiding potentially harmful contact. The technique is based on x-ray attenuation (usually in dual-energy mode), and is sensitive to the materials' different x-ray stopping power. This quantity varies with objects composition, density and x-ray energy. X-ray imaging is a fundamental tool for security screening, but it has some weaknesses. It is not uncommon that the x-ray attenuation properties of a non-threat material match those of a threat object, producing a false alarm. The rate of false alarms (1-specificity), together with the ability to correctly identifying targets (sensitivity), provide a metrics to compare different systems performances [1]. Higher specificity and sensitivity would lead to: faster security procedures, fewer operators employed and reduced stress for the users. Therefore, any technique which can improve current specificity and sensitivity standards is attractive.

X-ray phase contrast imaging (XPCI) is a recent development, which allows the detection of the changes in the phase of the x-rays in addition to their attenuation. The induced phase shift derives from a physical quantity different from attenuation. Therefore, measuring the phase shift provides access to information which is invisible to conventional x-ray systems. X-ray refraction (i.e. the derivative of the phase shift), appears as a small angular deviation (i.e. micro-radians) in x-ray direction, and it is strongest at detail edges. In certain cases, x-ray refraction can be detected when the x-ray attenuation is practically zero. An additional contrast accessible with XPCI is ultra-small angle x-ray scattering (USAXS; also known as dark-field), which is multiple x-ray refraction generated by details smaller than the system resolution [2-4]. USAXS information is complementary to absorption and refraction, providing clues on the microscale structure of the materials. USAXS has been exploited in different fields such as: mammography [5, 6], x-ray angiography with alternative contrast agents [7-9], lung imaging [10-12], kidney stone differentiation [13] and detection of defects in composite structures [14, 15].

The advantages of XPCI can also be exploited in baggage screening. In addition to the attenuation contrast, XPCI provides an enhanced contrast of the details' borders via the refraction signal, which improves object recognition [16].

Moreover, USAXS can be used to better characterize objects with a crystalline or quasi-crystalline structure, which can be confused with threat materials. The combination of USAXS with the attenuation properties could provide the fingerprint of a specific material. Therefore there is the potential for XPCI to improve specificity and sensitivity in baggage screening.

Edge Illumination (EI) [17] is one of the XPCI techniques which can provide USAXS as well as phase signals, and can be implemented with conventional x-ray sources [18]. In EI, small x-rays beams are created using a gold mask with small apertures placed before the sample (M1; see Figure 1). A second gold mask (M2), with correspondingly scaled apertures, is aligned in front of the detector. Each beamlet illuminates one pixel column of the detector. A sample placed between M1 and M2 will deviate the beamlets causing an intensity change at the detector pixels (Figure 1). Acquiring a series of images at different M1 x-positions enables the retrieval of the absorption, refraction and USAXS properties of the object.
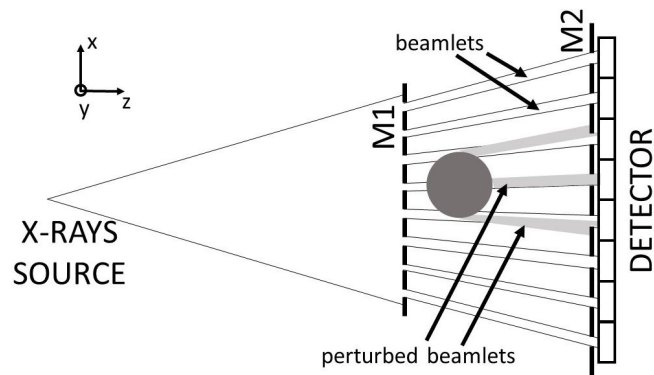

Figure 1 A schematic representation of the EI-XPCI setup. The pre-sample mask (M1) creates the x-ray beamlets, which pass through the apertures of the detector mask (M2). The object placed between M1 and M2 deviates the beamlets causing and intensity change on the detector.

EI is a relatively new technique which, up to now suffered from two main limitations which are common also to other XPCI approaches: 1- the field of view (FOV) was small (typically 5 x 5 cm^2), because of the limitations in the production of large optical elements; 2- the x-ray energy used is low because of the high aspect ratio required for the gold optical element at higher energies. Although there have been incremental improvements in this sense [19-21], a system providing simultaneously high energy and large FOV was not available till now.

In this contribution, we present the design of the first asymmetric mask EI-XPCI setup [22] optimized for baggage screening. The prototype was built in a collaboration between the University College London and Nikon Metrology (Tring, UK). For the first time, phase-based multimodal imaging (i.e. the capability of retrieving attenuation, refraction and USAXS contrasts simultaneously) is available together with a large FOV and high x-ray energies. The preliminary results obtained with this scanner will be presented.

2. MATERIALS AND METHODS

The ideal characteristics of an XPCI baggage screening system are: 1- high x-ray energy ($\geq$ 80 kV); 2- large FOV ($\geq$ 20 cm); 3- fast scanning ($\geq$ 0.2 m/s); 4- good quality for absorption, refraction and USAXS images. Monte Carlo simulations were used to design the system through a previously validated code [23], which uses the free software package McXtrace [24]. In order to fulfill the previously mentioned requirements, we investigated the effects on image quality of varying: magnification, aperture sizes, number of asymmetric periods introduced in M1. An important role is played by the masks gold thickness, which is supposed to stop all radiation outside the apertures. Since it is technically harder to create narrow apertures in thick gold layers (high aspect ratio), the larger the apertures the easier it is to make the gold thicker. Larger apertures also mean higher statistic and faster screening. On the other hand, larger apertures may decrease the image quality, mainly due to cross-talk between adjacent beamlets.

We simulated: four aperture sizes at the detector (15 µm, 20 µm, 30 µm, 40 µm), two magnification levels (M=1.33 and 1.25) with constant source to detector distance (2 m), and two tungsten spectrums (80 kV and 100 kV).

The following parameters were selected for the final design: M=1.33, and 21.4 μm and 28 μm aperture sizes for M1 and M2, respectively; four asymmetric points (with a shift of 10 μm from each other). To cover a large FOV (compared with previous EI setups) we combined, for each of the two masks (M1 and M2), three smaller masks (with sizes 5 x 1.2 cm^2 and 6.7 x 1.5 cm^2 for M1 and M2 respectively). Those three sub-masks were carefully aligned under an optical microscope, and fixed on a steel support. This solution allowed to reach a total FOV at the detector of 20 x 1.28 cm^2. An optical microscope photo of a M1 is shown in Figure 2a, where the groups of 4 shifted apertures are visible.

The x-ray source is a tungsten X-Tek 160 tube (80 μm focal spot) and the detector is a dual energy photon counting CdTe-CMOS (XCounter XC-FLITE FX2). It has 2048 x 128 squared pixels with 100 μm side, resulting in a FOV of 20.48x1.28 cm^2. Each of the two masks are mounted on a stack of four motors, which facilitate the alignment process. The baggage is scanned in front of the x-ray beam via a 50 cm range translator. This enables to scan large objects in a single acquisition. The system is assembled inside a lead shielded X-Tek NGI cabinet as shown in Figure 3a.

The retrieval of absorption, phase and USAXS is done using the following method. An intensity profile (illumination curve; IC) is measured by moving M1 across the x-ray beam (along the x-axis as in Figure 1). A total of 11 points equally spaced over one apertures period are collected without the sample. For each group of 4 adjacent pixels columns the resulting 44 points (11 per column) are fitted with a four-Gaussians curve (this featuring 12 parameters in total) plus an offset (a_3) (Equation 1; Figure 2b). This approach automatically includes the cross-talk between adjacent beamlets.

$$IC(x) = \sum_{i=1}^{4} \frac{a_{i0}}{\sqrt{2\pi a_{i2}^2}} Exp\left[-\frac{1}{2}\left(\frac{x - a_{i1}}{a_{i2}} \right)^2 \right] + a_3 \qquad (1)$$

An object is then scanned in front of M1 and synchronized with the detector continuous acquisition. The system resolution along the x-axis is defined by the stage speed times the detector framerate. It can be tuned from a minimum of 21.4 μm to several millimeters, while the highest resolution on the y-axis is determined by the effective pixel size (75 μm) or its multiples in *rebinned* mode. Following the formalism used before [25-27], the scanned object will modify each of the four Gaussians of Equation 1 by the same amount in terms of intensity (t_1, t_0), peak position (Δ_x) and width (σ), which are directly related to absorption, refraction and USAXS, respectively. Therefore the IC with the object can be fitted with the function in Equation 2.

$$f(x) = \sum_{i=1}^{4} \frac{t_1 a_{i0}}{\sqrt{2\pi\left(a_{i2}^2 + \sigma^2\right)}} Exp\left[-\frac{1}{2} \frac{(x - a_{i1} - \Delta_x)^2}{a_{i2}^2 + \sigma^2} \right] + t_0 a_3 \qquad (2)$$
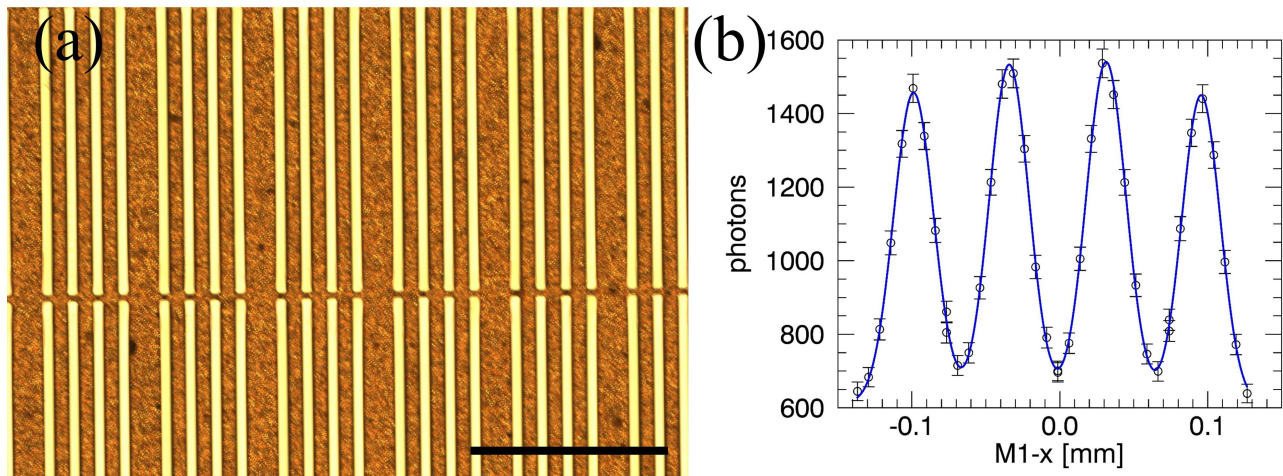

Figure 2 Detail of the pre-sample mask (M1) with the asymmetric apertures. The 4-points pattern is repeated so the images from corresponding lines belonging to different groups can be added to improve the image statistics (a) (scale bar 0.5 mm). Example of the ICs of 4 adjacent apertures, and the fits (blue line) obtained through equation 1 (b).
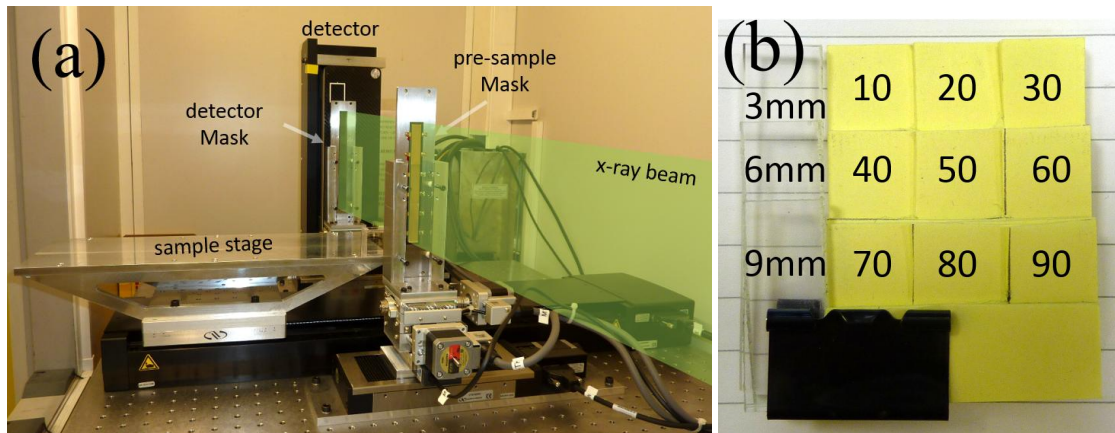
Figure 3 Photo of the setup (a). Photo of the sample used for the preliminary calibration (b). On the left hand side three steps of PMMA (3 mm, 6 mm and 9 mm) are visible, to the right of which nine steps of paper with increasing thickness (ranging from 10 to 90 sheets). Total size approximately 5 x 5 cm^2.

To test the system accuracy, we measured a sample with increasing amounts of paper (Figure 3b). Specifically, nine areas with increasing thickness of paper (ranging from 10 to 90 sheets, 1 sheet is approximately 90 μm thick) are assembled alongside three steps of PMMA (3 mm, 6 mm and 9 mm). The acquisition was run at 80 kV, 160 W, with a framerate of 1 Hz and an effective squared pixel size of 150 μm (using a rebin equal to 2 along the y-axis). The detector energy threshold was set to approximately split the beam spectrum in two images with comparable statistics. This modality allows obtaining low and high energy information through a single scan without the need for two separate beams. The acquisition took approximately 5 minutes. The relatively slow acquisition is due to having selected the lower possible framerate, since we wanted to test the system at the highest possible photon statistics. From the retrieved images of absorption (t_1) and USAXS (σ) we extracted 9 small region of interests inside each detail areas by extracting their mean and standard deviation.

Faster acquisitions are obtained by decreasing the resolution and the exposure time. As an example, images of a bag containing several everyday items (1 toothbrush, 1 toothpaste, 1 stick deodorant, 1 brush, 1 razor, 4 contact lenses containers, one small soap tablet and 1 small perfume bottle) are acquired. In this case, the x-ray tube was set to 100 kV, 160 W, the effective pixel was 300 μm and the framerate 16 Hz, resulting in a scanning speed of 5 mm/s.

3. RESULTS

In Figure 4 the retrieved USAXS values for PMMA and paper are shown vs the minus logarithm of the transmission (-log(t_1)). The low and high energy results are marked in red and blue, respectively. The lines represents the linear fit of the data showing a good linearity of the system response.

Figure 5 shows an example of the large FOV capabilities of the system. The retrieved images (absorption, refraction and USAXS) of a small bag are shown.
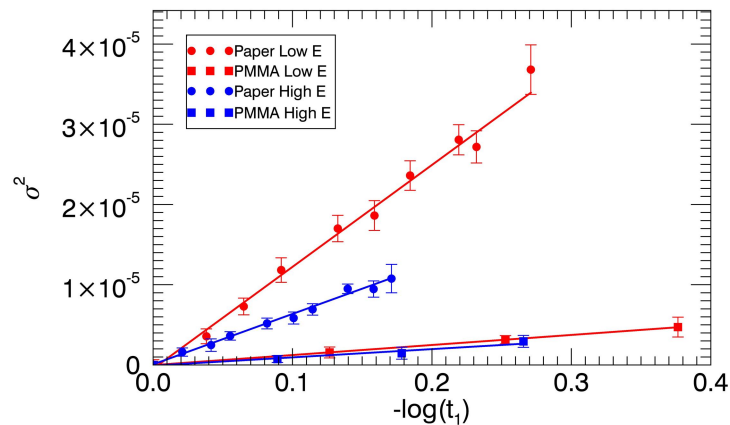
Figure 4 Scatter plot with attenuation on the x-axis and USAXS on the y-axis for the calibration sample. The points represent several thickness of paper and PMMA. Red and blue refer to low and high energy data respectively. The lines are the linear fits for the different materials and energy.
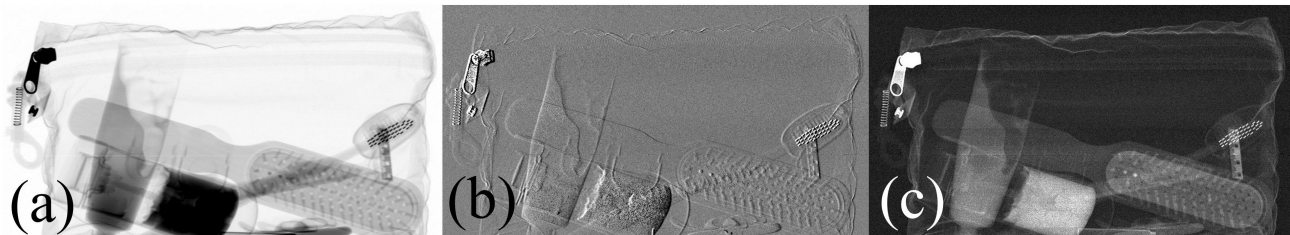

Figure 5 The three retrieved images of a bag containing several everyday items (size 25x15 cm^2): absorption (a), refraction (b) and USAXS (c).

4. CONCLUSIONS

The first high energy, large FOV XPCI system was presented. Quantitative values were retrieved from a non-threat test object. The setup can provide refraction and USAXS information, together with the conventional x-ray absorption image. Energy sensitivity is obtained via the dual energy single photon counting detector, without the need of an additional source/detector. The system provides 6 independent images from a single acquisition (absorption, refraction and USAXS at low and high x-ray energy). This multimodality/dual-energy capability will be exploited in baggage screening with the aim to improve specificity and sensitivity of threat detection.

ACKNOWLEDGEMENTS

REFERENCES

[1]   K. Wells, and D. A. Bradley, "A review of X-ray explosives detection techniques for checked baggage," Applied Radiation and Isotopes, 70(8), 1729-1746 (2012).

[2]   E. Pagot, P. Cloetens, S. Fiedler et al., "A method to extract quantitative information in analyzer-based x-ray phase contrast imaging," Applied Physics Letters, 82(20), 3421-3423 (2003).

[3]   L. Rigon, H. J. Besch, F. Arfelli et al., "A new DEI algorithm capable of investigating sub-pixel structures," Journal of Physics D: Applied Physics, 36(10 A), A107-A112 (2003).

[4]   M. N. Wernick, O. Wirjadi, D. Chapman et al., "Multiple-image radiography," Physics in Medicine and Biology, 48(23), 3875-3895 (2003).

[5]   Z. Wang, and M. Stampanoni, "Quantitative x-ray radiography using grating interferometry: A feasibility study," Physics in Medicine and Biology, 58(19), 6815-6826 (2013).

[6]   S. Grandl, K. Scherer, A. Sztrókay-Gaul et al., "Improved visualization of breast cancer features in multifocal carcinoma using phase-contrast and dark-field mammography: an ex vivo study," European Radiology, 25(12), 3659-3668 (2015).

[7]   F. Arfelli, L. Rigon, and R. H. Menk, "Microbubbles as x-ray scattering contrast agents using analyzer-based imaging," Physics in Medicine and Biology, 55(6), 1643-1658 (2010).

[8]   T. P. Millard, M. Endrizzi, N. Everdell et al., "Evaluation of microbubble contrast agents for dynamic imaging with x-ray phase contrast," Scientific Reports, 5, (2015).

[9]   A. Velroyen, M. Bech, A. Tapfer et al., "Ex vivo perfusion-simulation measurements of microbubbles as a scattering contrast agent for grating-based X-ray dark-field imaging," PLoS ONE, 10(7), (2015).

[10] M. Bech, A. Tapfer, A. Velroyen et al., "In-vivo dark-field and phase-contrast x-ray imaging," Scientific Reports, 3, (2013).

[11] A. Yaroshenko, T. Pritzke, M. Koschlig et al., "Visualization of neonatal lung injury associated with mechanical ventilation using x-ray dark-field radiography," Scientific Reports, 6, (2016).

[12] A. Yaroshenko, K. Hellbach, A. Ö. Yildirim et al., "Improved in vivo Assessment of Pulmonary Fibrosis in Mice using X-Ray Dark-Field Radiography," Scientific Reports, 5, (2015).

[13] K. Scherer, E. Braig, K. Willer et al., "Non-invasive Differentiation of Kidney Stone Types using X-ray Dark-Field Radiography," Scientific Reports, 5, (2015).

[14] M. Endrizzi, B. I. S. Murat, P. Fromme et al., "Edge-illumination X-ray dark-field imaging for visualising defects in composite structures," Composite Structures, 134, 895-899 (2015).

[15] T. Lauridsen, M. Willner, M. Bech et al., "Detection of sub-pixel fractures in X-ray dark-field tomography," Applied Physics A: Materials Science and Processing, 121(3), 1243-1250 (2015).

[16] K. Ignatyev, P. Munro, R. Speller et al., "X-ray phase contrast imaging with coded apertures for next generation baggage scanning systems." 292-295.

[17] A. Olivo, and R. Speller, "A coded-aperture technique allowing x-ray phase contrast imaging with conventional sources," Applied Physics Letters, 91(7), (2007).

[18] M. Endrizzi, P. C. Diemoz, T. P. Millard et al., "Hard X-ray dark-field imaging with incoherent sample illumination," Applied Physics Letters, 104(2), (2014).

[19] J. Meiser, M. Willner, T. Schröter et al., "Increasing the field of view in grating based X-ray phase contrast imaging using stitched gratings," Journal of X-Ray Science and Technology, 24(3), 379-388 (2016).

[20] T. Thüring, M. Abis, Z. Wang et al., "X-ray phase-contrast imaging at 100 keV on a conventional source," Scientific Reports, 4, (2014).

[21] A. Sarapata, M. Willner, M. Walter et al., "Quantitative imaging using high-energy X-ray phase-contrast CT with a 70 kVp polychromatic X-ray spectrum," Optics Express, 23(1), 523-535 (2015).

[22] M. Endrizzi, A. Astolfo, F. A. Vittoria et al., "Asymmetric masks for laboratory-based X-ray phase-contrast imaging with edge illumination," Scientific Reports, 6, (2016).

[23] T. P. Millard, M. Endrizzi, P. C. Diemoz et al., "Monte Carlo model of a polychromatic laboratory based edge illumination x-ray phase contrast system," Review of Scientific Instruments, 85(5), (2014).

[24] E. Bergbäck Knudsen, A. Prodi, J. Baltser et al., "McXtrace: A Monte Carlo software package for simulating X-ray optics, beamlines and experiments," Journal of Applied Crystallography, 46(3), 679-696 (2013).

[25] M. Endrizzi, and A. Olivo, "Absorption, refraction and scattering retrieval with an edge-illumination-based imaging setup," Journal of Physics D: Applied Physics, 47(50), (2014).

[26] M. Endrizzi, D. Basta, and A. Olivo, "Laboratory-based X-ray phase-contrast imaging with misaligned optical elements," Applied Physics Letters, 107(12), (2015).

[27] F. A. Vittoria, G. K. N. Kallon, D. Basta et al., "Beam tracking approach for single-shot retrieval of absorption, refraction, and dark-field signals with laboratory x-ray sources," Applied Physics Letters, 106(22), (2015).